

# The distance to the Orion Nebula

K. M. Menten<sup>1</sup>, M. J. Reid<sup>2</sup>, J. Forbrich<sup>1,2</sup>, and A. Brunthaler<sup>1</sup>

<sup>1</sup> Max-Planck-Institut für Radioastronomie, Auf dem Hügel, D-53121 Bonn, Germany  
e-mail: kmenten, brunthala@mpi-fr-bonn.mpg.de

<sup>2</sup> Harvard-Smithsonian Center for Astrophysics, 60 Garden Street, Cambridge, MA 02138, USA  
e-mail: reid, jforbrich@cfa.harvard.edu

Received; accepted

## ABSTRACT

We have used the Very Long Baseline Array to measure the trigonometric parallax of several member stars of the Orion Nebula Cluster showing non-thermal radio emission. We have determined the distance to the cluster to be  $414 \pm 7$  pc. Our distance determination allows for an improved calibration of luminosities and ages of young stars. We have also measured the proper motions of four cluster stars which, when accurate radial velocities are measured, will put strong constraints on the origin of the cluster.

**Key words.** Stars: pre-main sequence, Radio continuum: stars

## 1. Introduction

The rich Orion Nebula Cluster, the best-studied of all star clusters, is an important “laboratory” for stellar astrophysics and early stellar evolution. Most of its  $\approx 3500$  stars formed within the past  $2 \cdot 10^6$  yr. The most massive stars, the  $\theta^1$  “Trapezium” system, have evolved close to the main sequence (Hillenbrand 1997; Palla & Stahler 1999), while many lower mass members are still pre-main sequence (PMS) stars. The dominant Trapezium star  $\theta^1 C$  (spectral type O5–O7) is responsible for the excitation of the spectacular Orion Nebula (ON) Messier 42, the only ionized nebula visible with the naked eye and extensively studied since the seventeenth century (Herczeg 1998), since the 1950s at all wavelengths.

The youngest stars in the region are found in the nearby Becklin-Neugebauer/Kleinmann-Low (BN/KL) region. The BN/KL region is a very dense part of Orion Molecular Cloud-1, which is located just a fraction of a parsec behind the ONC (Zuckerman 1973; Genzel & Stutzki 1989) and is home to at least one high-mass star that is currently forming (Orion-I) (Churchwell et al. 1987; Menten & Reid 1995; Reid et al. 2007).

Given the importance of the ONC and the BN/KL region for the study of star formation and early stellar evolution, knowledge of their distance,  $D$ , is of great interest. For example, luminosities are a critical constraint on stellar evolution models, which deliver stellar masses and cluster ages. Note that a luminosity determination depends on the square of the distance! In addition, accurate distances are needed to determine binary-star separations, to convert angular motions to velocities, and to estimate stellar mass-loss rates.

Distance estimates for the ONC from the early 1900s ranged from 2000 pc based on apparent magnitudes and colors of faint stars in the ON’s neighborhood, to 180 pc, based on the moving cluster method using stars widely distributed around the ON (Pickering 1917; Kapteyn 1918). Later, luminosity-based distance estimates of the Trapezium stars were plagued by the poorly known and spatially variable extinction within the nebula and ranged from 540 pc to 300 pc (Trumpler 1931; Minkowski

1946). Various distance estimates from the 1960s through the 1980s, summarized in Jeffries (2007), used optical and near-infrared (NIR) photometry and color-magnitude diagrams to yield  $347 \text{ pc} < D < 483 \text{ pc}$ .

Uncertain extinction corrections and variations of extinction across the Nebula, quantified, e.g., by Bohlin & Savage (1981), may have led to part of the large spread in distances published over the last few decades. Thus, measuring distance by methods that are independent of photometry is highly desirable. Comparing radial velocities and proper motions for samples of stars for which both could be measured has yielded distances from 380 pc to 520 pc (Johnson 1965; Strand 1958). Recent modeling of the rotational properties of ONC pre-main-sequence stars has given  $D = 440 \pm 34$  pc for a sample of 74 stars, which falls to  $392 \pm 32$  pc when stars with accretion disks are excluded (Jeffries 2007). Very Long Baseline Interferometry (VLBI) determinations of the internal proper motions of “clouds” of water vapor ( $\text{H}_2\text{O}$ ) masers in the BN/KL region led to another photometry-independent distance estimate of  $D = 480 \pm 80$  pc (Genzel et al. 1981).

Very recently, Kraus et al. (2007) used multiple visual and NIR interferometric observations to determine two orbital solutions for the  $\theta^1 C$  close binary system. One invokes a distance of  $434 \pm 12$  pc and the other  $387 \pm 11$  pc. The existing data do not allow favoring one over the other.

It is apparent from the above summary that there is disagreement of at least  $\pm 10\%$  among the various methods of estimating the distance to the ONC, which leads directly to uncertainties of  $\pm 20\%$  for luminosities. Clearly a much more accurate distance for the ONC would be a fundamental advance for stellar astrophysics.

The “gold standard” for astronomical distance measurements is the trigonometric parallax, which uses the ancient surveying technique of triangulation. For astronomical applications, the Earth’s orbit is used as the length scale for one leg of the triangle, and the angular displacement of an object (relative to very distant sources) directly yields the object’s distance. Optically, only a single ONC member star has a trigonometric parallax,  $361_{-87}^{+168}$  pc obtained from the Hipparcos astrometric

Star	$\alpha_{J2000}$	$\delta_{J2000}$	SIMBAD	H97	JW88	COUP
GMR						
A	05 35 11.80318	-5 21 49.2504	-	-	-	450
12	05 35 15.82615	-5 23 14.1296	$\theta^1$ A <sub>1</sub> Ori	680		745
G	05 35 17.95028	-5 22 45.5058	MT Ori	815	567	932
F	05 35 18.37143	-5 22 37.4342	V1229 Ori	852	589	965

**Table 1.** Non-thermally emitting stars in the ONC detected by the VLBA. The first column gives the radio source designation from Garay et al. (1987) and the second and third columns the J2000 position determined by us and calculated for the midpoint of our observations (epoch 2006.46). The identifications in the fourth through seventh columns come from the SIMBAD database and Hillenbrand (1997); Jones & Walker (1988); Getman et al. (2005).

satellite (Bertout et al. 1999); but this measurement is not accurate enough for most astrophysical applications. Extraordinarily high astrometric accuracies can now be achieved with VLBI techniques. Recently, trigonometric parallax distances to the ON have been reported to be  $437 \pm 19$  pc from water masers in the BN/KL region using the VERA (VLBI Exploration of Radio Astrometry) array (Hirota et al. 2007) and  $389^{+24}_{-21}$  pc from an ONC star (GMR A; see below) using the NRAO<sup>1</sup> Very Long Baseline Array (VLBA) (Sandstrom et al. 2007). These measurements represent a significant advance for the distance to the Nebula, but the values still differ by  $48 \pm 30$  pc.

Using the VLBA, source positions can now be measured with an accuracy of  $\sim 10$  micro-arcseconds ( $\mu$ as) relative to very distant quasars. Recently, VLBA observations of methanol and water masers have yielded trigonometric parallax distances for the star-forming region W3OH in the Perseus spiral arm of the Milky Way of 2.0 kpc with  $\approx 2\%$  accuracy (Xu et al. 2006; Hachisuka et al. 2006). After completing these measurements, we started an astrometric program with the VLBA in order to determine trigonometric parallaxes for radio-emitting stars in the ONC.

The Orion Nebula is known to contain about 90 compact radio stars, either associated with the ONC or with dust-embedded sources in the nearby BN/KL region (Garay et al. 1987; Churchwell et al. 1987). The emission from many of these sources is thermal in nature, either resulting from external ionization of circumstellar material (protoplanetary disks or “proplyds”) by the UV radiation of  $\theta^1$  C Ori, or from internal UV sources exciting hypercompact ionized regions. However, more than 30 sources have shown significant time variability and/or emit x-rays (Felli et al. 1993; Zapata et al. 2004). Probably these are non-thermal radio emitters, making them suitable sources for VLBA parallax measurements<sup>2</sup>.

## 2. Observations and data analysis

### 2.1. Observations

Our observations with the VLBA were conducted on 2005 September 25, 2006 March 02, 2006 September 09, and 2007

<sup>1</sup> The National Radio Astronomy Observatory (NRAO) is operated by Associated Universities, Inc., under a cooperative agreement with the National Science Foundation.

<sup>2</sup> The VLBA images containing stars presented in this paper have an rms noise level around  $0.1$  mJy beam<sup>-1</sup>. In a  $2 \times 1$  milliarcsecond FWHM synthesized beam this corresponds to a brightness temperature of  $8.6 \cdot 10^5$  K.

March 6. These dates well sample the maximum extent of the Earth’s orbit as viewed by the source. We designed the observations to measure only the Right Ascension (R.A.) component of the trigonometric parallax signature, because this component has about twice the amplitude of the Declination (Decl.) component and the angular resolution of the VLBA for this source is about two times better in R.A. than in Decl.

The pointing position for the VLBA antennas for the Orion Nebular Cluster was  $(\alpha, \delta)_{J2000} = 05^{\text{h}}35^{\text{m}}15.^{\text{s}}0, -05^{\circ}22'45''$ . We chose the compact extragalactic source J0541–054 as the phase-reference from the International Celestial Reference Frame (ICRF) catalog (Ma et al. 1998), adopting its position to be  $(\alpha, \delta)_{J2000} = 05^{\text{h}}41^{\text{m}}38.^{\text{s}}083384 \pm 0.^{\text{s}}000019, -05^{\circ}41'49''.42839 \pm 0.''00046$ . We alternately observed J0541–054 and the Orion position, switching sources every 40 seconds over a period of 8 hours during each epoch. The observing setup used 8 intermediate frequency (IF) bands of 8 MHz, with 4 detecting right and 4 left circular polarization. The center frequency of the bands was 8437 MHz and together they spanned a total 32 MHz in each polarization.

The data were correlated with the VLBA correlator in Socorro, NM, with an averaging time of 0.131 seconds. The position offsets of the ONC stars from the pointing position are small relative to the FWHM of an individual VLBA antenna’s primary beam ( $5'.3$ ). However, we had to correlate the data in three passes, owing to the large interferometer fringe-rate differences among them. Three correlator phase-center positions were used  $(\alpha, \delta)_{J2000} = 05^{\text{h}}35^{\text{m}}11.^{\text{s}}8022, -05^{\circ}21'49''.229, 05^{\text{h}}35^{\text{m}}16.^{\text{s}}2890, -05^{\circ}23'16''.575,$  and  $05^{\text{h}}35^{\text{m}}18.^{\text{s}}3706, -05^{\circ}22'37''.436$ . Bandwidth smearing limits the effective field-of-view to about 22 arcseconds about each correlator position. Within this field of view, amplitude decorrelation is less than 10% on our longest interferometer baselines.

### 2.2. Calibration

Most of the data calibration steps are standard and described in the on-line documentation of the NRAO AIPS software package<sup>3</sup>. Below we discuss additional calibrations that allow improved astrometric accuracy.

The main source of systematic error for cm-wave phase-referenced observations is uncompensated interferometric delays introduced by the Earth’s atmosphere and ionosphere, and we conducted supplementary observations that allowed us to correct for these effects (Reid & Brunthaler 2004). These observations were done by spreading the 8 left-circularly polarized IF bands to sample about 500 MHz of bandwidth. Approximately 15 ICRF sources whose positions are known to better than 1 mas were observed over a span of about 40 minutes at the beginning, middle and end of the Orion observations. The effects of ionospheric delays were removed by using total electron content values from GPS data. Also, data were corrected for the best Earth’s orientation parameter values, as the VLBA correlator by necessity uses preliminary values available at correlation. Broad-band interferometer residual delays were estimated and modeled as owing to clock drifts and zenith atmospheric delays. The phase-referenced data was then corrected for these effects.

Electronic delay and phase differences among the different IF bands were removed by measuring them on a strong calibrator, 0530+133, and correcting the data. Then the data on the rapid-switching reference source, J0541–054, from all IF bands were combined and tables of antenna-based interferometer phase

<sup>3</sup> See the AIPS “cookbook” under <http://www.nrao.edu/aips>.

versus time were generated. These phases were interpolated to the times of the Orion data and subtracted from that data.

All calibrations were applied to the data and synthesis maps were made using the AIPS task IMAGR. Typical dirty-beam FWHM sizes were 2.1 by 0.9 mas elongated in the north-south (NS) direction. Positions of both the reference source and the Orion stars were determined by fitting 2-dimensional Gaussian brightness distributions to the images using JMFIT.

### 2.3. Imaging

We searched for compact radio emission from a total of 23 stars, but only detected the four stars in Table 1 above a secure ( $> 5\sigma$ ) detection threshold of  $\approx 1$  mJy. The locations of these stars within the core of the ONC are shown in Fig. 1, using the stellar designations from Garay, Moran & Reid (GMR, Garay et al. 1987). The star GMR A has no optical counterpart, but has long been known to be a variable radio source, whose emission was found by VLBA observations to be very compact:  $\sim 1$  milli-arcsecond (mas). In 2003 January a remarkable outburst of several days duration was observed at millimeter and radio wavelengths, during which the source’s 86 GHz flux density rose more than 10-fold (Bower et al. 2003). Near infrared (NIR) photometry and spectroscopy indicate that GMR A is a deeply embedded, very young (T Tauri) star with more than 20 mag of visual extinction. In x-rays, GMR A is characterized as a “flare source” and the x-ray data indicate an absorbing column of  $4 \cdot 10^{22} \text{ cm}^{-2}$ , which is consistent with the extinction derived from the NIR data (Feigelson et al. 2002).

The other stars detected, GMR 12, GMR F, and GMR G, are coincident with optically visible stars and are undoubtedly ONC members. The later two stars are listed as  $\pi 1925$  and  $\pi 1910$ , respectively, in the classic Parenago catalog (Parenago 1954). GMR 12 is the binary companion of the Trapezium star  $\theta^1$  A Ori (named  $\theta^1$  A<sub>2</sub> Ori). This 0.''2 separation binary system has recently been resolved by NIR speckle interferometry (Petr et al. 1998; Weigelt et al. 1999). (The primary,  $\theta^1$  A<sub>1</sub> Ori (B0.5 V), itself is a spectroscopic binary with a cooler companion.) GMR12 has been detected previously with VLBI observations (Felli et al. 1989, 1991; Garrington et al. 2002).

Three of our four stars were detected at all four epochs; GMR G was not detected on the first epoch owing to source variability. Our observations delivered the positions listed in Table 1 with an estimated precision of about 0.13 mas in R.A. and 0.28 mas in Decl. relative to the extragalactic reference source. Absolute position uncertainties are dominated by the  $\approx 0.5$  mas uncertainty in the ICRF position of the reference source. Our positions are in excellent agreement with the values determined by Gómez et al. (2005) using the Very Large Array within their larger errors.

Single component JMFIT solutions of our reference source, 0541–054, for each epoch yield an elongated elliptical Gaussian component with position angles, PAs, between 145 and 158 degrees (east of north) that is barely resolved. JMFIT delivers deconvolved sizes between 0.8 and 1.6 mas for the major axis and between 0.3 and 0.4 for the minor axis. This evokes the possibility of a core-jet structure. Note, that to first order, an evolving jet would contribute to the proper motion, but not to the parallax. Further note that our parallax essentially derives from the east-west (EW) data.

To quantitatively study the effect that source structure might have on the determinations of 0541–041’s centroid position we conducted 2 (Gaussian) component fits using JMFIT. In this case the task delivers a very compact stronger component of size

$< 0.7$  mas and a weaker elongated component with a major axis of size  $\approx 4$  mas. For the latter’s minor axis JMFIT returns upper limits between 0.05 and 0.2 mas for the first three epochs, while it has broadened to 2 mas in the fourth epoch. This “broadening” may indicate more complex source structure emerging. For the compact component, which almost certainly represents the QSO’s core, we found small deviations from the 1 Gaussian fit centroid position of  $-0.057, -0.037, -0.064, \text{ and } +0.005$  mas in R.A. direction and  $-0.084, +0.036, +0.002, \text{ and } +0.002$  mas in Decl. direction for the four epochs, which contribute to the error floors discussed in §3.

In Table 2, we present the stars’ positions together with the fitted peak intensities,  $S_p$ , (brightness values) and integrated flux densities,  $S$ . A comparison of the numerical values of  $S_p$  and  $S$  shows that all sources at most epochs appear only marginally resolved, if at all. Since the sources appear more resolved when they have low flux densities and do hardly appear resolved at all when their flux densities are highest, we ascribe this apparent resolving of sources to residual calibration uncertainties that affect low signal-to-noise cases relatively the most.

### 3. Results – Parallax and proper motion determinations

We used our positions as input data for a least-squares fitting program, which modeled the data as the sum of the sinusoidal parallax term and a proper motion term. The parallax term is entirely determined by one parameter ( $\pi$ ), since the Earth’s orbit and source directions are well known. The proper motion term requires two parameters for each coordinate: an angular offset and speed. The first four lines of Table 3 give the best fit parallaxes and proper motions for all four stars individually. In Fig. 2 we plot the positions of the 4 stars versus time with the best fit parallax and proper motion models. Since all stars are at the same distance, within measurement accuracy, we also present a combined solution in which we simultaneously solve for a single parallax parameter and separate proper motions for the three stars detected in all four epochs (see final line of Table 3 and Fig. 3).

For this fit, an error “floor” was added to the formal position uncertainties in order to account for systematic errors, resulting mostly from unmodeled atmospheric delays and variations in the calibrator positions; see §2.2. The error floors for the R.A. and Decl. data (0.12 and 0.27 mas, respectively) were separately adjusted to bring the reduced  $\chi^2$  value (per degree of freedom) to unity in each coordinate. Without the error floors the reduced  $\chi^2$  values were 3.7 in R.A. and 7.5 in Decl. (per degree of freedom), respectively. After applying these weighting factors, the best fit parallax was  $2.415 \pm 0.040$  mas, corresponding to a distance of  $414.0 \pm 6.8$  pc. Both approaches, the single source average and the joint solution fit, give similar results, and we adopt the joint solution value, i.e., a distance of  $414 \pm 7$  pc.

We also determined a parallax including the data for GMR G. For this fit, we obtained  $\pi = 2.448 \pm 0.042$  mas, corresponding to  $D = 408.5 \pm 7.0$  pc. This is within  $1\sigma$  with the 414.0 pc determined above, a value which we retain as our best estimate for the reason that of all sources GMR G consistently showed the lowest flux densities making it the most vulnerable to systematic errors. This is reflected by the fact that the formal error of the fit that included GMR G is not smaller than that of the three source only fit.

Our distance, 414 pc, is the most accurate measurement for the Orion region, having an uncertainty of only 1.7%. Both of the

Star	Epoch	$S_p$ (mJy b <sup>-1</sup> )	$S$ (mJy)	$\alpha_{J2000}$	$\delta_{J2000}$	$\theta_{\text{maj}}$ (mas)	$\theta_{\text{min}}$ (mas)	PA (deg)
GMR A	1	0.9(0.1)	0.9(0.3)	05 35 11.803276(6)	-05 21 49.24884(20)	< 1.6	< 0.8	161(3)
	2	2.1(0.1)	2.8(0.3)	05 35 11.803031(2)	-05 21 49.25059(6)	1.1(3)	0.6(2)	171(30)
	3	10.7(0.1)	13.1(0.2)	05 35 11.803409(1)	-05 21 49.25063(2)	1.5(2)	0.5(1)	170(4)
	4	10.8(0.1)	14.9(0.2)	05 35 11.803135(1)	-05 21 49.25219(1)	0.8(1)	0.4(2)	71(8)
GMR 12	1	2.1(0.1)	6.9(0.5)	05 35 15.826115(5)	-05 23 14.12875(9)	3.1(3)	–	58(7)
	2	14.4(0.1)	16.8(0.2)	05 35 15.825945(1)	-05 23 14.12943(1)	1.0(1)	0.3(1)	163(3)
	3	4.9(0.1)	6.8(0.2)	05 35 15.826430(1)	-05 23 14.12961(3)	1.6(2)	0.7(1)	173(6)
	4	4.8(0.1)	5.5(0.2)	05 35 15.826262(1)	-05 23 14.13120(2)			
GMR G	1	< 0.24						
	2	1.1(0.1)	1.5(0.2)	05 35 17.950071(2)	-05 22 45.45702(9)	1.4(4)	< 0.7	19(20)
	3	2.0(0.1)	2.2(0.2)	05 35 17.950564(2)	-05 22 45.45477(7)	< 1.5	–	9(40)
	4	4.7(0.1)	5.1(0.2)	05 35 17.950357(1)	-05 22 45.45364(2)	< 0.7	< 0.6	34(25)
GMR F	1	1.0(0.1)	1.9(0.2)	05 35 18.371521(4)	-05 22 37.43477(14)	2.1(5)	< 0.9	162(9)
	2	6.8(0.1)	7.3(0.2)	05 35 18.371255(1)	-05 22 37.43470(2)	< 0.6	< 0.4	16(43)
	3	26.8(0.2)	29.2(0.3)	05 35 18.371659(1)	-05 22 37.43379(1)	1.4(1)	< 0.1	167(3)
	4	2.4(0.1)	3.1(0.2)	05 35 18.371415(1)	-05 22 37.43403(3)	< 1.0	< 0.9	124(35)

**Table 2.** Fitted values for the four ONC stars determined by Gaussian fitting. Left to right we list name, epoch, peak intensity (brightness), total flux density, R.A., Decl., fitted major and minor axis and position angle. Formal  $1\sigma$  uncertainties in the last listed digit returned by JMFIT are given in parentheses. For R.A. values with smaller uncertainties than  $1 \mu\text{second}$ , 1 is given for display reasons. Epochs 1 through 4 correspond to 2005 September 25, 2006 March 2, 2006 September 9, and 2007 March 6. Absolute position accuracy is limited the  $\pm 0.5$  mas ICRF position accuracy of the phase-reference source, J0541–054. GMR G was not detected at epoch 1. The quoted brightness is a  $3\sigma$  upper limit. For some fits JMFIT did not return a value for the major or minor axis, for some only an upper limit.

trigonometric parallaxes mentioned above (Hirota et al. 2007; Sandstrom et al. 2007) are consistent with our value within their larger uncertainties of about  $\pm 20$  pc.

#### 4. Discussion

Our accurate distance is approximately 10% lower than the 450 pc distance often assumed for the ONC. Since luminosity is proportional to distance squared, our distance implies that luminosities of the ONC member stars have been over-estimated by nearly 20%. Reducing luminosities affects theoretical investigations of the ONC’s star formation history (Palla & Stahler 1999). Age and mass estimates from stellar evolution models are discussed in the literature. We have used an online tool (Siess et al. 2000; Siess 2001) which allows one to calculate the change in age and mass,  $M$ , for pre-main-sequence stars with masses between  $0.1$  and  $7 M_\odot$  and to trace lines for given masses in a luminosity versus temperature diagram (“PMS tracks”). For low-mass ( $M < 1 M_\odot$ ), cool ( $< 5000$  K) stars, the vertical tracks indicate little change in mass from a reduced luminosity and we find little (at most a few percent) difference in mass for a given luminosity. However, ages are significantly affected and become 20 to 30% larger by using our accurate distance. The same happens for higher mass stars, except that masses are affected, too, and drop by up to 10% for stars with  $7 M_\odot$ .

The proper motions of the four stars are in the heliocentric equatorial reference frame. We transform them into a Galactocentric Cartesian reference frame ( $U, V, W$ ), where  $U$  points toward the Galactic center,  $V$  points toward the direction of Galactic rotation, and  $W$  points toward the North Galactic Pole. To correct for the Sun’s motion, we used the latest values derived from the analysis of Hipparcos data (Dehnen & Binney 1998). For the distance to the Galactic center and the circular rotation speed in the Solar Neighborhood, we assume the IAU values of  $8.5$  kpc and  $220 \text{ km s}^{-1}$ , respectively.

Source	$\pi$ (mas <sup>-1</sup> )	$D$ (pc)	$\mu_x$ (mas y <sup>-1</sup> )	$\mu_y$ (mas y <sup>-1</sup> )
GMR A	2.390(0.104)	418.4(18.2)	+1.82(0.09)	-2.05(0.18)
GMR 12	2.393(0.053)	417.9(9.2)	+4.82(0.09)	-1.54(0.18)
GMR G	–	–	+4.29(0.17)	+3.33(0.37)
GMR F	2.462(0.051)	406.1(8.4)	+2.24(0.09)	+0.66(0.18)
Mean	2.425(0.035)	412.4(6.0)		
Joint	2.415(0.040)	414.0(6.8)		

**Table 3.** Fitted distances and proper motions. The first column lists the radio source designation. The second and the third columns give the parallax and distance estimates derived from a fit to the measured positions in which the parallax and the proper motions in R.A. and Decl. direction (listed in columns four and five) were left as free parameters. A proper motion of  $1.0 \text{ mas y}^{-1}$  corresponds to a velocity of  $2.0 \text{ km s}^{-1}$  at a distance of 414 pc. The fifth line gives the weighted mean parallax and distance and their standard errors of the mean, and the sixth line gives the results of a combined solution, where only one parallax was fitted to the measurements of GMR A, GMR 12, and GMR F.

The calculated  $U, V$ , and  $W$  values are dependent on the assumed radial velocities of our stars. Unfortunately, no accurate radial velocity values have been published for GMR 12, F, and G. With the heliocentric radial velocity determined for GMR A of  $+14 \pm 5 \text{ km s}^{-1}$  (Bower et al. 2003), we calculate  $U = +9.6 \pm 4.2 \text{ km s}^{-1}$ ,  $\Delta V = -3.8 \pm 2.6 \text{ km s}^{-1}$  (slower than Galactic rotation), and  $W = +5.5 \pm 1.7 \text{ km s}^{-1}$ , where  $\Delta V$  is the difference between  $V$  and the rotation speed of the Milky Way at the position of the ONC. For a rotation curve that is constant with Galactocentric radius, as appears to be the case near the Sun, the assumed value of the rotation speed does not significantly affect  $\Delta V$ .

If accurate radial velocities for all our program stars could be determined, e.g., with IR spectroscopy, such measurements combined with our proper motions could constrain dynamical scenarios for the formation of the Orion complex, which is located at the large distance of 19.4 degrees (140 pc) below the Galactic plane. To explain this puzzling offset one theory invokes a high velocity cloud colliding with the Galactic plane 6  $10^7$  y ago, sweeping up and compressing material in the process, and subsequently oscillating about the plane (Franco et al. 1988).

The proper motions of our four stars have a dispersion of 1.5 and 2.6 mas  $y^{-1}$  in R.A. and Decl. These values, which correspond to 3 and 5 km  $s^{-1}$ , respectively, are somewhat uncertain because of small number statistics, but are significantly larger than velocity dispersions of 1 km  $s^{-1}$  found from optical proper motion studies (Jones & Walker 1988; van Altena et al. 1988). One explanation for this difference may be that three or our four stars lie far from the cluster center and, thus, could be responding to a larger enclosed mass than the bulk of the stars nearer to the center.

*Acknowledgements.* We would like to thank Thomas Preibisch for discussions and Mark McCaughrean for an electronic version of his K-band image. We are grateful to the referee for perceptive comments that helped to improve this paper. Andreas Brunthaler was supported by the Priority Programme 1177 of the Deutsche Forschungsgemeinschaft.

## References

- Bertout, C., Robichon, N., & Arenou, F. 1999, A&A, 352, 574  
 Bohlin, R. C. & Savage, B. D. 1981, ApJ, 249, 109  
 Bower, G. C., Plambeck, R. L., Bolatto, A., et al. 2003, ApJ, 598, 1140  
 Churchwell, E., Wood, D. O. S., Felli, M., & Massi, M. 1987, ApJ, 321, 516  
 Dehnen, W. & Binney, J. J. 1998, MNRAS, 298, 387  
 Feigelson, E. D., Broos, P., Gaffney, III, J. A., et al. 2002, ApJ, 574, 258  
 Felli, M., Massi, M., & Catarzi, M. 1991, A&A, 248, 453  
 Felli, M., Massi, M., & Churchwell, E. 1989, A&A, 217, 179  
 Felli, M., Taylor, G. B., Catarzi, M., Churchwell, E., & Kurtz, S. 1993, A&AS, 101, 127  
 Franco, J., Tenorio-Tagle, G., Bodenheimer, P., Rozyczka, M., & Mirabel, I. F. 1988, ApJ, 333, 826  
 Garay, G., Moran, J. M., & Reid, M. J. 1987, ApJ, 314, 535  
 Garrington, S. T., van Langevelde, H. J., Campbell, R. M., & Gunn, A. 2002, in Proceedings of the 6th EVN Symposium, ed. E. Ros, R. W. Porcas, A. P. Lobanov, & J. A. Zensus, 259–+  
 Genzel, R., Reid, M. J., Moran, J. M., & Downes, D. 1981, ApJ, 244, 884  
 Genzel, R. & Stutzki, J. 1989, ARA&A, 27, 41  
 Getman, K. V., Flaccomio, E., Broos, P. S., et al. 2005, ApJS, 160, 319  
 Gómez, L., Rodríguez, L. F., Loinard, L., et al. 2005, ApJ, 635, 1166  
 Hachisuka, K., Brunthaler, A., Menten, K. M., et al. 2006, ApJ, 645, 337  
 Herczeg, T. 1998, Acta Historica Astronomiae, 3, 246  
 Hillenbrand, L. A. 1997, AJ, 113, 1733  
 Hirota, T., Bushimata, T., Choi, Y. K., et al. 2007, ArXiv e-prints, 705  
 Jeffries, R. D. 2007, MNRAS, 159  
 Johnson, H. M. 1965, ApJ, 142, 964  
 Jones, B. F. & Walker, M. F. 1988, AJ, 95, 1755  
 Kapteyn, J. C. 1918, ApJ, 47, 104  
 Kraus, S., Balega, Y. Y., Berger, J.-P., et al. 2007, A&A, 466, 649  
 Ma, C., Arias, E. F., Eubanks, T. M., et al. 1998, AJ, 116, 516  
 Menten, K. M. & Reid, M. J. 1995, ApJ, 445, L157  
 Minkowski, R. 1946, PASP, 58, 356  
 Palla, F. & Stahler, S. W. 1999, ApJ, 525, 772  
 Parenago, P. P. 1954, Trudy Gosudarstvennogo Astronomicheskogo Instituta, 25, 1  
 Petr, M. G., Coude Du Foresto, V., Beckwith, S. V. W., Richichi, A., & McCaughrean, M. J. 1998, ApJ, 500, 825  
 Pickering, W. H. 1917, Harvard College Observatory Circular, 205, 1  
 Reid, M. J. & Brunthaler, A. 2004, ApJ, 616, 872  
 Reid, M. J., Menten, K. M., Greenhill, L. J., & Chandler, C. J. 2007, ApJ, 664, 950  
 Sandstrom, K. M., Peek, J. E. G., Bower, G. C., Bolatto, A. D., & Plambeck, R. L. 2007, ArXiv e-prints, 706  
 Siess, L. 2001, in Astronomical Society of the Pacific Conference Series, Vol. 243, From Darkness to Light: Origin and Evolution of Young Stellar Clusters, ed. T. Montmerle & P. André, 581–+  
 Siess, L., Dufour, E., & Forestini, M. 2000, A&A, 358, 593  
 Strand, K. A. 1958, ApJ, 128, 14  
 Trumpler, R. J. 1931, PASP, 43, 255  
 van Altena, W. F., Lee, J. T., Lee, J.-F., Lu, P. K., & Upgren, A. R. 1988, AJ, 95, 1744  
 Weigelt, G., Balega, Y., Preibisch, T., et al. 1999, A&A, 347, L15  
 Xu, Y., Reid, M. J., Zheng, X. W., & Menten, K. M. 2006, Science, 311, 54  
 Zapata, L. A., Rodríguez, L. F., Kurtz, S. E., & O'Dell, C. R. 2004, AJ, 127, 2252  
 Zuckerman, B. 1973, ApJ, 183, 863

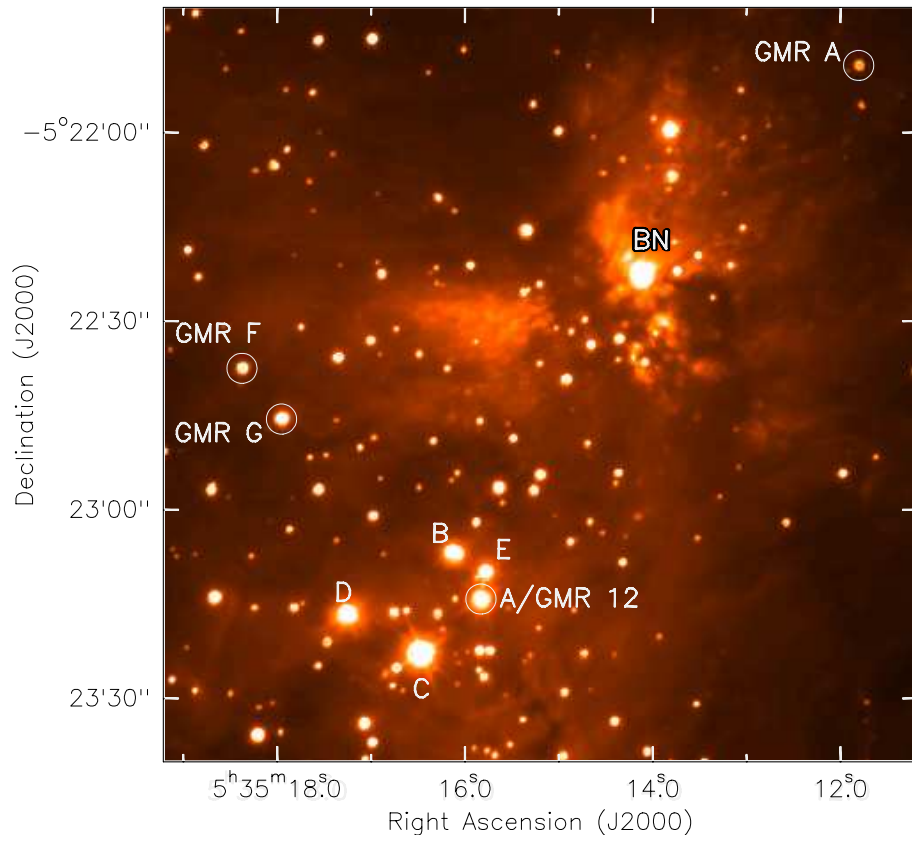


**Fig. 1.** Infrared K-band image of the ONC and the BN/KL region. (courtesy M. McCaughrean). The Trapezium stars (A, B, C, D & E) and the BN object are labeled. Our program stars (GMR A, GMR F, GMR G & GMR 12) are labeled and encircled. The image was taken with the ESO Very Large Telescope.

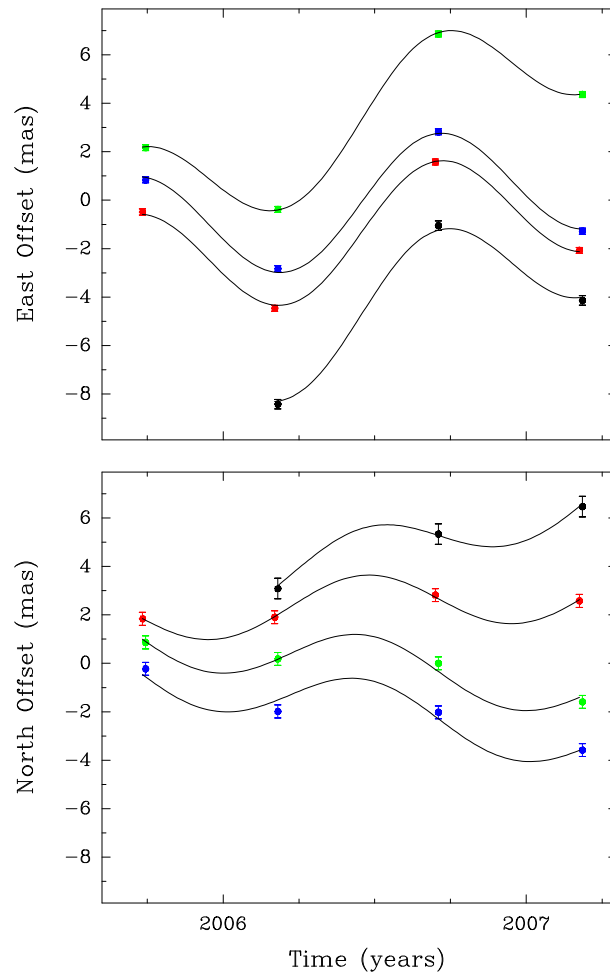


**Fig. 2.** Position versus time for GMR G (black), GMR F (red), GMR 12 (green), and GMR A (blue). The top and bottom panels show the eastward (R.A.  $\cos(\text{Decl.})$ ) and northward (Decl.) offsets, respectively. For each star the best fit distance from the correlator phase-center position has been removed and then offset for clarity. Also plotted are best fit models. For each star, except GMR G, the model is characterized by five parameters: one for the parallax and two for the proper motion speed and position offset for each coordinate. For GMR G, which was detected at only 3 epochs, the parallax value was fixed at the “joint-solution” value (2.415 mas; see Fig. 3) and only the proper motion parameters were adjusted.

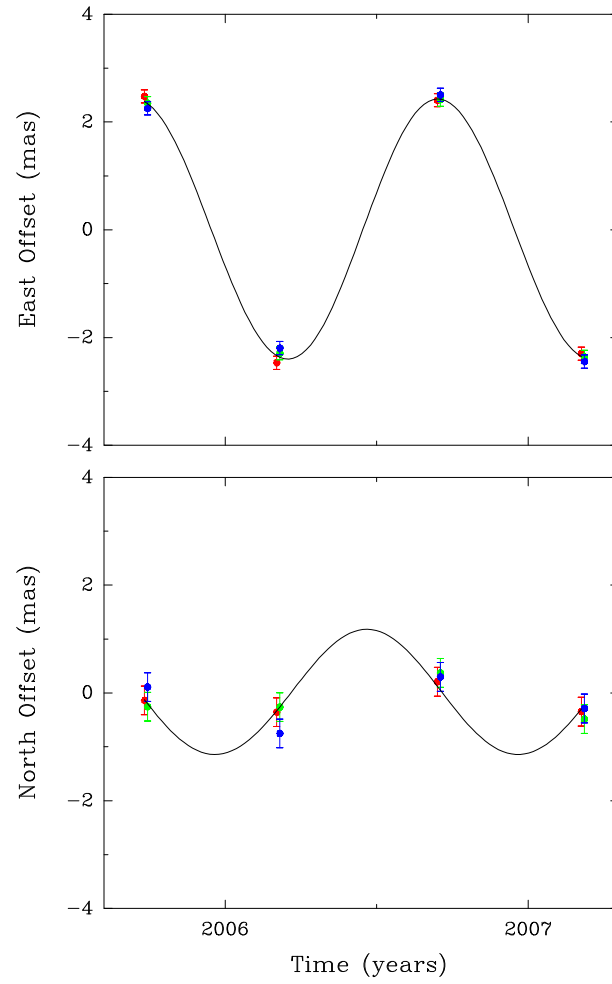


**Fig. 3.** Joint parallax fit for the 3 stars detected at all 4 epochs using position versus time data for GMR F (red), GMR 12 (green), and GMR A (blue). The top and bottom panels show the eastward and northward offsets, respectively. For each star the best fit proper motions have been subtracted. The best fit parallax was  $2.415 \pm 0.040$  mas, corresponding to a distance of  $414.0 \pm 6.8$  pc.